Applied Catalysis B: Environmental 306 (2022) 121116

Contents lists available at ScienceDirect

Applied Catalysis B: Environmental

journal homepage: www.elsevier.com/locate/apcatb

Unravelling the synergy in platinum-nickel bimetal catalysts designed by atomic layer deposition for efficient hydrolytic dehydrogenation of ammonia borane

Jiankang Zhang [a,*], Xiuhui Zheng [b], Wenlong Yu [c], Xiang Feng [b,*], Yong Qin [a,d]

[a] Interdisciplinary Research Center of Biology & Catalysis, School of Life Sciences, Northwestern Polytechnical University, Xi'an 710072, PR China
[b] State Key Laboratory of Heavy Oil Processing, China University of Petroleum, Qingdao 266580, PR China
[c] State Key Laboratory Base of Eco-Chemical Engineering, College of Chemical Engineering, Qingdao University of Science and Technology, Qingdao 266042, PR China
[d] State Key Laboratory of Coal Conversion, Institute of Coal Chemistry, Chinese Academy of Sciences, Taiyuan 030001, PR China

ARTICLE INFO

Keywords:
Atomic layer deposition
Bimetal synergy
Pt-Ni interfacial sites
Hydrogen evolution activity
Kinetic-isotopic analyses

ABSTRACT

Bimetal catalysis has been one of the major categories in heterogeneous catalysis field, and the efficient and durable catalysts can be well achieved by the bimetal synergy. Herein we report a remarkable achievement of both dehydrogenation activity of ammonia borane and durability by controllably engineering Pt-Ni interfacial sites via the Pt and the following NiO atomic layer deposition strategy, which can also realize the controllable synthesis of other Pt-M (M=Co, Cu, Fe and Zn) bimetal catalysts. Multiple characterization techniques, kinetic-isotopic analyses and density functional theory calculations were employed to unravel the nature of the Pt-Ni synergy. Experimental and theoretical results reveal that the decoration of nickel species on the Pt nanoparticles constructing the targeted Pt-Ni interfacial sites could lower the reaction activation energy, promote the adsorption, activation and dissociation of H_2O molecules, and facilitate the desorption of hydrogen atoms, resulting in the doubly enhanced activity with a turnover frequency value of 751.6 mol_{H2} mol_{Pt}^{-1} min^{-1} and the remarkably improved durability. Our work offers an alternative and general strategy for the rational design of bimetal catalysts with specific interfacial structure and provides fundamental guidance for in-depth understanding of the bimetal synergy.

1. Introduction

Supported platinum (Pt)-based catalyst is one of the most investigated and most efficient catalysts in both scientific research and industrial application fields [1–7]. In recent decades, tremendous efforts have been devoted to investigating the structure-performance relationship so as to develop the Pt-based catalysts with high efficiency and durability [1–7]. Engineering the particle size and distribution of Pt metal and strengthening the interaction between metal and support are the widely applied strategies to develop high-efficiency and high-durability Pt-based catalysts [1–9], while another efficient strategy is the combination of Pt with other metals/metal oxides to make full use of the bimetal synergy [10–23]. Although the bimetal catalysts have been widely reported and excellent catalytic performances have been achieved in various heterocatalytic reactions (e.g., dehydrogenation, hydrogenation and photo/electrochemical reactions) [10–23], mechanistic insight into the bimetal synergy nature and structure-performance relationship is still challenging, which is mainly hampered by the lack of effective strategy to realize the precise regulation toward the catalyst structures (especially for the bimetal interfacial structure). Therefore, precisely designing and constructing the catalysts with specific structures are the prerequisite to unravel the bimetal synergy and catalytic mechanism.

Atomic layer deposition (ALD) is an advanced and alternative technique for the precise design and controllable synthesis of the catalytic materials. It can facilely achieve the precise tuning of the catalyst structures such as metal nanoparticle size, distribution and interfacial engineering [21–33]. Herein we report the new PtNix/CNTs (x is the number of NiO ALD cycles and CNTs represent carbon nanotubes) bimetal catalysts with controllable Pt-Ni interfacial sites achieved by ALD technique to investigate the nature of Pt-Ni synergy in the hydrolysis reaction of ammonia borane (AB), which is difficult to achieve by

* Corresponding authors.
E-mail addresses: zhangjiankang@nwpu.edu.cn (J. Zhang), xiangfeng@upc.edu.cn (X. Feng).

https://doi.org/10.1016/j.apcatb.2022.121116
Received 18 November 2021; Received in revised form 11 January 2022; Accepted 18 January 2022
Available online 19 January 2022

the traditional methods. For comparison, other bimetal catalysts such as PtCo/CNTs, PtCu/CNTs and PtFe/CNTs were also synthesized by ALD technique. The addition of the second metal oxide species has a crucial influence on the catalytic property, and especially the PtNi/CNTs catalysts exhibit remarkably boosted hydrogen evolution activity and robust durability because of the synergistic effects between Pt and Ni. Multiple characterization techniques, the kinetic-isotopic measurements as well as the density functional theory (DFT) calculations were adopted to unravel the structure-performance relationship of PtNix/CNTs (x = 0, 5, 10, 20, 40 and 100) catalysts and the synergistic catalytic mechanism.

2. Experimental

2.1. Catalyst preparation

The pretreated CNTs by concentrated HNO_3 solution were chosen as the supports to prepare the catalysts in a homemade ALD reactor [21]. For the monometallic Pt/CNTs catalysts, the (methylcyclopentadienyl) trimethylplatinum ($MeCpPtMe_3$) and O_3 were used as Pt precursor and reactant gas, respectively. The Pt content corresponding to the number of Pt ALD cycle was kept constant (20 cycles, ca. 8.03 wt%), and the Pt:M ratio was adjusted by varying the metal oxide ALD cycles. For the typical bimetal PtNix/CNTs (x = 5, 10, 20, 40 and 100 ALD cycles) catalysts, the second species (NiO) was deposited onto the Pt/CNTs with bis(cyclopentadienyl)nickel ($NiCp_2$) as the NiO precursor. $MeCpPtMe_3$ and $NiCp_2$ contained in stainless steel bubbler were heated to 60 °C and 68 °C respectively to provide enough vapor pressure, and the deposition temperature was set at 280 °C. For comparison, PtCo/CNTs, PtFe/CNTs, PtCu/CNTs and PtZn/CNTs bimetal catalysts were also prepared. The PtCo/CNTs, PtFe/CNTs and PtCu/CNTs catalysts were prepared by depositing CoO_x, Fe_2O_3 or CuO onto Pt/CNTs with bis(cyclopentadienyl)cobalt(II), ferrocene and bis(2,2,6,6-tetramethyl-3, 5-heptanedionato)copper(II) as the corresponding precursors reacting with O_3. The PtZn/CNTs catalysts were prepared by depositing ZnO onto Pt/CNTs with diethylzinc and deionized H_2O as reactants. The number of the metal oxide ALD cycle is 20 unless otherwise specified.

2.2. Catalyst characterizations

X-ray powder diffraction (XRD) patterns were collected on a Bruker D8 Advance X-ray powder diffractometer with Cu Kα radiation (λ = 0.154 nm). The transmission electron microscopy (TEM) and high-resolution TEM images were taken with a JEOL-2100F instrument operated at 200 kV. The high-angle annular dark-field scanning TEM images and energy-dispersive X-ray spectroscopy mapping were collected on a Tecnai G2-F20 S-Twin and FEI-Themis Z instrument operated at 200 kV and 300 kV, respectively. The X-ray photoelectron spectra measurements were carried out with an ESCALab-250Xi X-ray photoelectron spectrometer (Al Kα, 1486.6 eV). The metal content of the catalysts was measured by inductively coupled plasma mass spectrometry. The X-ray absorption spectroscopy experiments were conducted on the BL14W1 beamline of the Shanghai Synchrotron Radiation Facility.

2.3. Catalytic activity measurements

Hydrolytic dehydrogenation of AB: A certain amounts of catalysts and 10 mL of deionized H_2O were added into a round-bottom flask, then 1.5 mmol of AB was added into the flask under stirring conditions (n_{Pt}/n_{AB}=0.0016). The volume of evolved hydrogen was measured in a water-filled graduated burette system by recording the displacement of water level. For the durability experiments, another equivalent of AB was added into the reactor when the remaining H_2 in the reaction system was exhausted after the completion of reaction.

Selective hydrogenation of 5-hydroxymethylfurfural (HMF): The selective hydrogenation reactions of HMF were performed in a 50 mL stainless steel autoclave reactor. Typically, HMF (0.5 mmol), the catalysts (10 mg), and the ethanol solvent (20 mL) were loaded into the autoclave. The reaction temperature and pressure are kept at 60 °C and 2 MPa respectively. After the completion of the reaction, the reaction reactant and products were analyzed and quantified by gas chromatographic mass spectrometry (GC-MS, Thermo Scientific TRACE 1300).

3. Results and discussion

3.1. Catalyst characterizations

The PtNi/CNTs bimetal catalysts were synthesized by sequentially conducting Pt and NiO ALD process (Fig. 1a), in which the number of Pt-Ni interfacial sites can be well-controlled by facilely changing the number of NiO ALD cycles. Fig. 1b gives the typical transmission electron microscopy (TEM) image of the as-prepared PtNi20/CNTs catalysts. The bimetal PtNi nanoparticles are uniformly dispersed on the CNT supports (also see Fig. 2 and S1), and the average particle size of the PtNi20/CNTs catalysts is approximately 2.2 nm (inset in Fig. 1b), which is slightly larger than that of the monometallic Pt/CNTs counterparts (Fig. S2) [21]. This can be ascribed to the deposition growth of NiO onto/next to Pt nanoparticles resulting in the formation the slightly larger PtNi bimetal nanoparticles. From the high-resolution TEM (HRTEM) image of the PtNi20/CNTs catalysts (Fig. 1c), Pt and NiO are closely contacted. The measured d-spacing of the nanoparticle is about 0.223 nm corresponding to the Pt(111) plane, and the lattice spacing of about 0.241 nm can be ascribed to the NiO(111) plane [33]. The bimetal catalysts were also characterized by high-angle annular dark-field scanning TEM (HAADF-STEM) and energy-dispersive X-ray spectroscopy (EDS) mapping (Fig. 2), which again confirm the homogeneous distribution of the bimetal nanoparticles on CNTs.

Fig. 3a presents the X-ray powder diffraction (XRD) patterns of the monometallic Pt/CNTs and bimetal PtNix/CNTs catalysts. The diffraction peaks at around 26.2, 43.0, and 54.1° correspond to the (002), (100) and (004) reflections of graphite CNTs, respectively. The weak diffraction peak at around 39.4° could be well-indexed as the Pt(111) crystal plane, indicating the small size and high dispersion of the Pt nanoparticles [33], which is consistent with the above TEM results (Figs. 1 and 2). While no diffraction peak related to NiO or metallic Ni is detected, and this can be ascribed to the high dispersion of nickel species on the CNTs. Fig. 3b is the X-ray absorption near-edge spectroscopy (XANES) spectra of the Pt/CNTs, PtNi20/CNTs, reference Pt foil and PtO_2. The white line intensity of PtNi20/CNTs decreases slightly compared with that of Pt/CNTs, and this should be ascribed to the interaction between Pt and Ni modifying the electronic structure of Pt, which can be further verified by the X-ray photoelectron spectra (XPS) results. From the XPS survey spectra of the monometallic Pt/CNTs and bimetal PtNix/CNTs catalysts (Fig. 3c), the peaks of C, O, Pt and Ni are all detected (also see Figs. S3 and S4), which again confirms the achievement of deposition growth of Pt and NiO on CNT supports. Fig. 3d displays the Pt 4f XPS spectra of the five catalysts, and the deposition of NiO on Pt/CNTs reduces the Pt 4f binding energy, which suggests the electron transfer from NiO to Pt and results in the increased electron density of Pt in the PtNi/CNTs catalysts [33]. This can be further verified by the gradual changes of Ni 2p binding energy shifting to the higher positions (Fig. 3e). Besides, the deposition of NiO on Pt/CNTs also results in the decrease of Pt 4f peak intensity, indicating the partial decoration of NiO on Pt nanoparticles, and correspondingly the Ni 2p peak intensity and Ni contents increase monotonely (from 0 to 7.9 at%, Fig. 3c-f). These results demonstrate that NiO is decorated on/next to the Pt nanoparticles constructing the unique Pt-Ni interfaces, and the interaction between them would further influence the catalytic performance.

3.2. Catalyst evaluation and kinetics-isotopic analyses

The catalytic performance of the finely designed and synthesized

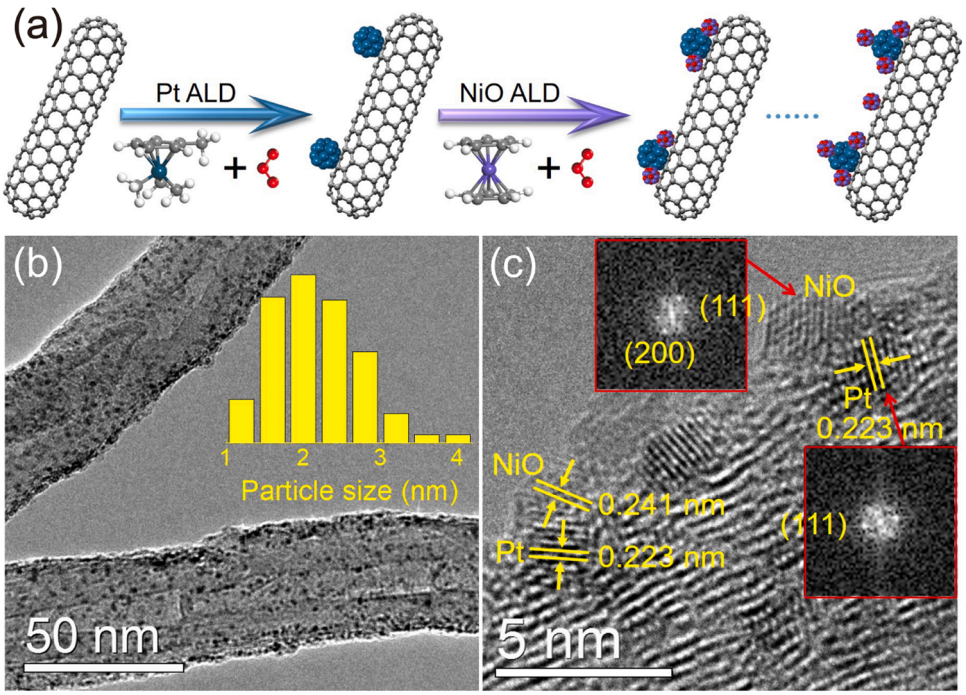

Fig. 1. (a) Schematic illustration of the synthesis of the PtNix/CNTs catalysts. The typical TEM (b) and HRTEM (c) images of the as-synthesized PtNi20/CNTs bimetal catalysts (Inset in panel b: the corresponding histogram of Pt particle size distribution). The number of NiO ALD cycles is 20 unless otherwise specified. The balls in gray, greyish-white, red, navy blue and purple represent carbon, hydrogen, oxygen, platinum and nickel, respectively.

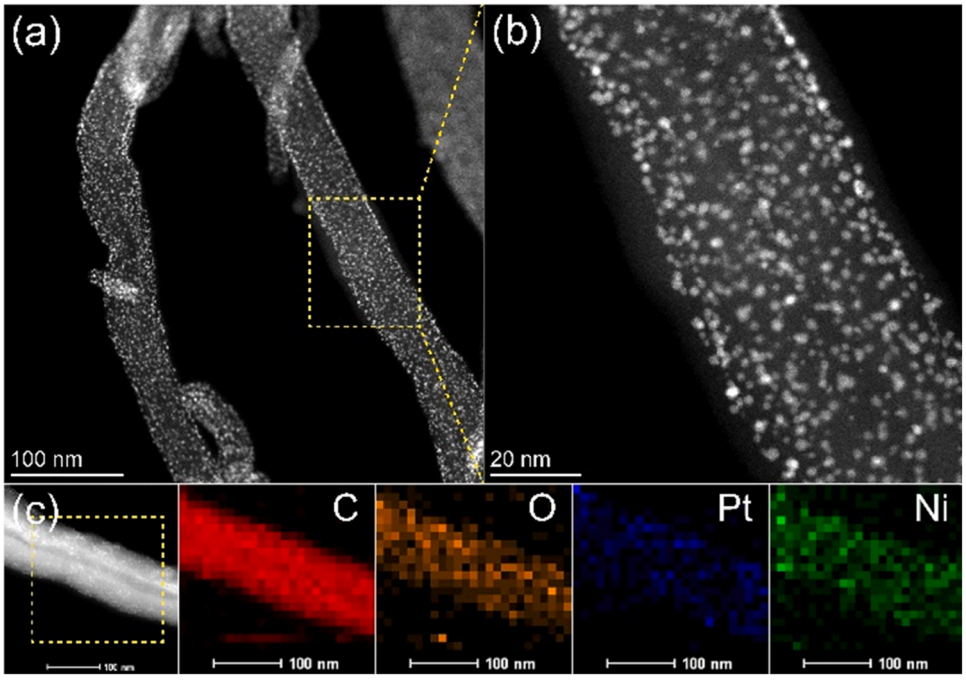

Fig. 2. Low and high magnification of the (a-c) HAADF-STEM images of the as-prepared PtNi20/CNTs catalysts and the corresponding EDS elemental mapping images of the rectangle area in panel (c) for C, O, Pt and Ni, respectively.

PtNix/CNTs catalysts by ALD, with controllable Pt-Ni interfacial sites, were evaluated in the hydrolytic dehydrogenation reaction of AB (a typical structure-sensitive reaction) [12–18,34–46]. As presented in Fig. 4a, the as-synthesized Pt-based catalysts are highly active presenting the almost linear H_2 evolution curves. When using the monometallic Pt/CNTs as catalysts, the reaction can be completed in 5 min. While for the as-prepared Ni20/CNTs reference catalysts (Fig. S5), only trace conversion (about 0.9%) is obtained in the initial 5 min under the same reaction conditions. To our delight, the bimetal PtNi/CNTs catalysts exhibit remarkably enhanced hydrogen evolution activity and the catalytic activity for hydrogen is strongly dependent on the NiO cycle numbers (i.e., numbers of interfacial sites), as shown in Fig. 4a-c. Only slight enhancement is observed for the catalytic activity of hydrogen evolution when the NiO ALD cycle is 5. However, the catalytic activity

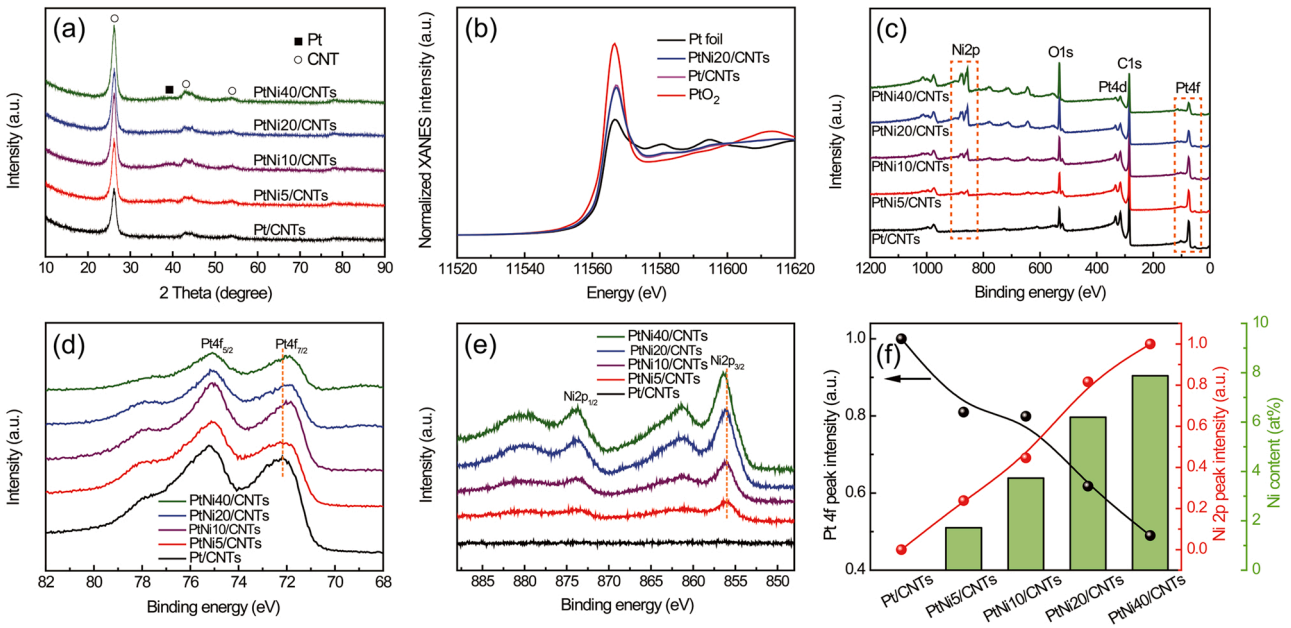

Fig. 3. (a) XRD patterns of the monometallic Pt/CNTs and bimetal PtNix/CNTs catalysts. (b) Pt Ledge XANES spectra of the Pt/CNTs, PtNi20/CNTs, Pt foil and PtO_2. (c) XPS survey, (d) Pt 4f and (e) Ni 2p spectra of the five catalysts. (f) The corresponding peak intensity changes and Ni contents of the five catalysts.

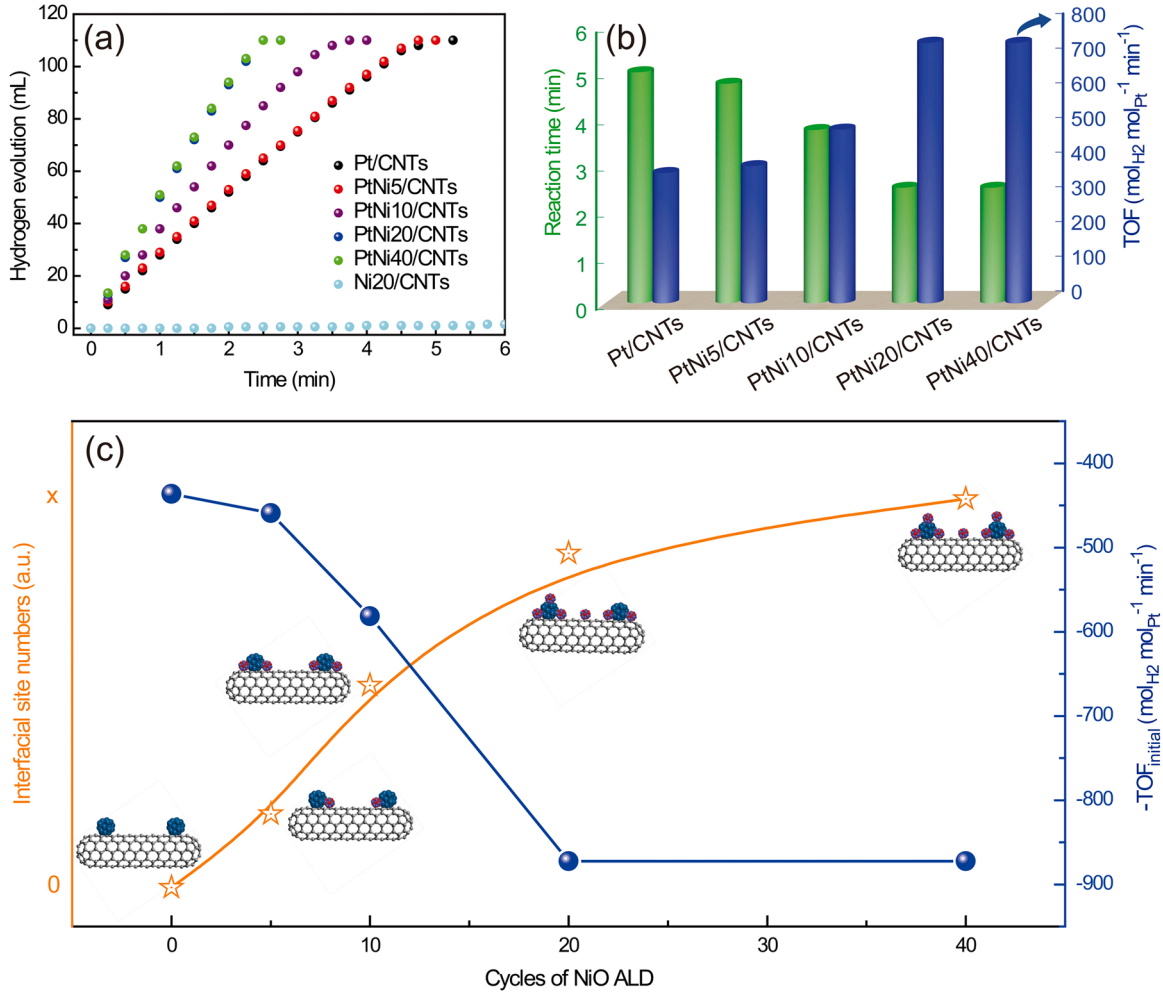

Fig. 4. (a) Volume of hydrogen evolved versus reaction time for hydrolytic dehydrogenation of AB at 25 °C catalyzed by the PtNix/CNTs and Ni20/CNTs catalysts. (b) The time needed to complete the reaction and TOF values of the PtNix/CNTs catalysts. (c) Pt-Ni interfacial site numbers and the initial reaction rates versus NiO ALD cycles.

has been doubled when the NiO ALD cycles increase to 20 presenting a turnover frequency (TOF, calculated based on the Pt molecules) value of 751.6 $mol_{H2}{\cdot}mol_{Pt}^{-1}$ min^{-1} for the optimized PtNi20/CNTs catalysts, and this value is higher than that of most of the Pt-based catalysts reported in the typical literature (Table S1) [38]. While further increasing the NiO ALD cycles (to 40 cycles) almost does not result in the enhancement of the hydrogen evolution activity (Fig. 4a-c). These results indicate that the catalytic activity can be well-regulated by varying the number of Pt-Ni interfacial sites, and that the potential Pt-Ni synergy is responsible for the remarkable enhancement of hydrogen evolution activity.

To gain in-depth understanding of the synergistic catalytic mechanism of Pt-Ni in the hydrolytic dehydrogenation reaction, the kinetic and isotopic experiments were conducted. The hydrogen evolution rates increase remarkably with increasing the reaction temperatures. The values of the reaction activation energy (E_a) over the catalysts can be determined from the corresponding Arrhenius plots (Figs. S6 and 5a), which are approximately 58.2, 52.4, 46.0, 44.8 and 46.8 kJ mol^{-1}, respectively. In other words, the addition of nickel species could obviously lower the reaction E_a. Furthermore, the isotopic experiments were also conducted to directly compare the kinetic isotope effect (KIE, $KIE=k_H/k_D$) values of the catalysts (Fig. S7), which is a powerful metric for the investigation of the rate-determining step (RDS) of a reaction. The calculated KIE values of the five catalysts are 4.0, 3.2, 2.2, 2.9 and 2.9, respectively (Fig. 5b), indicating that the activation and dissociation of H_2O molecules, i.e., the cleavage of O-H bond in H_2O molecules, should be involved in the RDS for the catalysts [16,17]. Note that all the bimetal catalysts afford lower KIE values compared with the monometallic counterparts, suggesting that the addition of nickel species can further promote the activation and dissociation of H_2O molecules, and this is also verified by the following DFT results.

For comparison, we also synthesized other bimetal catalysts and evaluated the catalytic activity and durability of the catalysts. As shown in Fig. 6a and b, the addition of CoO_x, similar to NiO, can also remarkably enhance the hydrogen evolution activity, while the addition of CuO leads to the limited enhancement of the hydrogen evolution activity. In contrast, the addition of ZnO or Fe_2O_3 results in the dramatic decrease of the hydrogen evolution activity. Durability is another vital evaluation criterion for the performance of the catalysts. Therefore, the durability tests were also conducted for the PtNi/CNTs and PtCo/CNTs catalysts with excellent activity (versus Pt/CNTs, Fig. 6c and d). The durability is relatively poor for the Pt/CNTs catalysts, i.e., the H_2 cannot be able to completely released in the fifth catalytic cycles (Fig. 6c), and there is obvious agglomeration and deformation for the nanoparticles of the recycled catalysts [21]. Although the PtCo/CNTs catalysts also exhibit much enhanced hydrogen evolution activity, the durability of the catalysts is still unsatisfactory (i.e., deactivate quickly) and the nanoparticles also deform and agglomerate seriously after six catalytic cycles. However, the PtNi/CNTs catalysts not only exhibit excellent hydrogen evolution activity, but also present much better durability than Pt/CNTs and PtCo/CNTs catalysts (Fig. 6c and d). The morphology and size of the PtNi nanoparticles can still be well preserved even after six catalytic cycles (Fig. 6e and S8), accounting for the excellent durability of the PtNi/CNTs catalysts. The adsorption of poisonous B-containing by-products on the catalyst surfaces resulting in the partial coverage of the metal active sites as well as the metal leaching should be the main reasons that lead to the some decreases of the catalytic activity in the continuous recycle tests (Fig. S9 and Table S2).

The above XPS results (Fig. 3c-e) have indicated that the introduction of NiO leads to the electron transfer from NiO to Pt resulting in the electron enrichment state of Pt (Fig. 6f). A similar case is also found for the PtFe/CNTs catalysts (Fig. 6f and S10), however, the catalysts display the dramatically decreased hydrogen evolution activity in comparison with Pt/CNTs catalysts. This could be ascribed to different capability to activate H_2O molecules for nickel and iron species. While the addition of cobalt oxides results in the shifts of Pt4f binding energy to the higher position for the PtCo/CNTs catalysts (Fig. 6f), and the catalysts still present much enhanced hydrogen evolution activity. The XANES results also indicate the different shift directions after introduction of nickel and cobalt oxides (Fig. S11). These results indicate that the modification of electron states of Pt (electron-deficient or electron-rich states, Fig. 6f) may not be the primary reason that leads to the different catalytic activity and durability of the bimetal catalysts. In other words, the catalytic performance is likely determined by the structural effect (i.e., the constructed Pt-M interfacial sites, Fig. 6g), because AB hydrolysis reaction is a typical structure-sensitive reaction. The catalytic performance is closely related to the kinds of additives, and the constructed PtNi/CNTs catalysts with suitable interfacial sites presenting both excellent hydrogen evolution activity and robust durability. Additionally, it should be noted that NiO is almost inactive for the catalytic hydrolysis reaction of AB. Even though the activity of the active metallic Ni is not a circumstance to that of noble metal Pt [38–43]. However, the addition of small amount of nickel species (ca. 6.2 at%) can result in the double increase of the hydrogen evolution activity, suggesting that the enhancement of the catalytic activity is not the simple superposition of the contribution of the two species. That is to say, the potential Pt-Ni synergy should be responsible for the enhancement of the hydrogen evolution activity and durability. Theoretically, when the highly active Pt metal is partially covered by the much less/inactive NiO, the hydrogen evolution activity of the catalysts would be decreased. However, the catalytic results have been proved that it is not the case for the PtNi/CNTs catalysts. Considering the specific structure of the designed catalysts with controllable Pt-Ni interfaces, the interfacial sites should play a crucial role enhancing the catalytic performances [21,47,48].

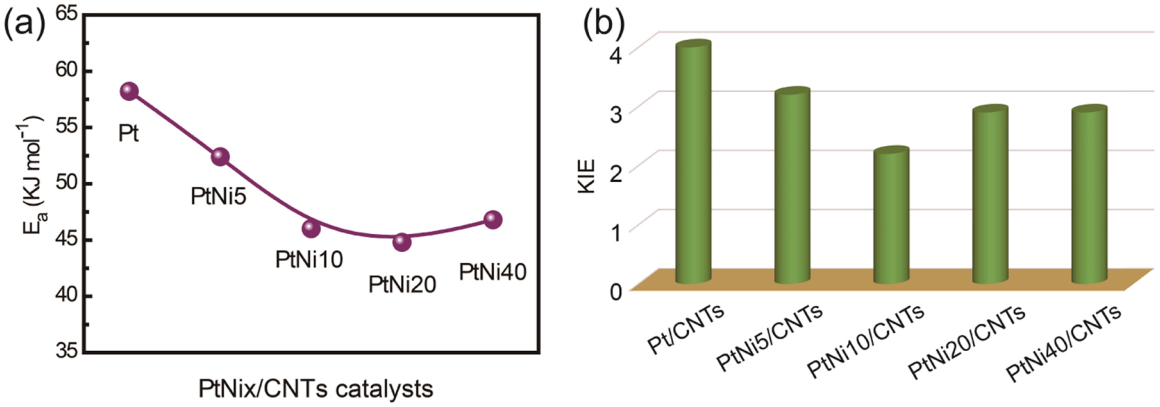

Fig. 5. (a) Reaction E_a and (b) KIE values of the catalysts.

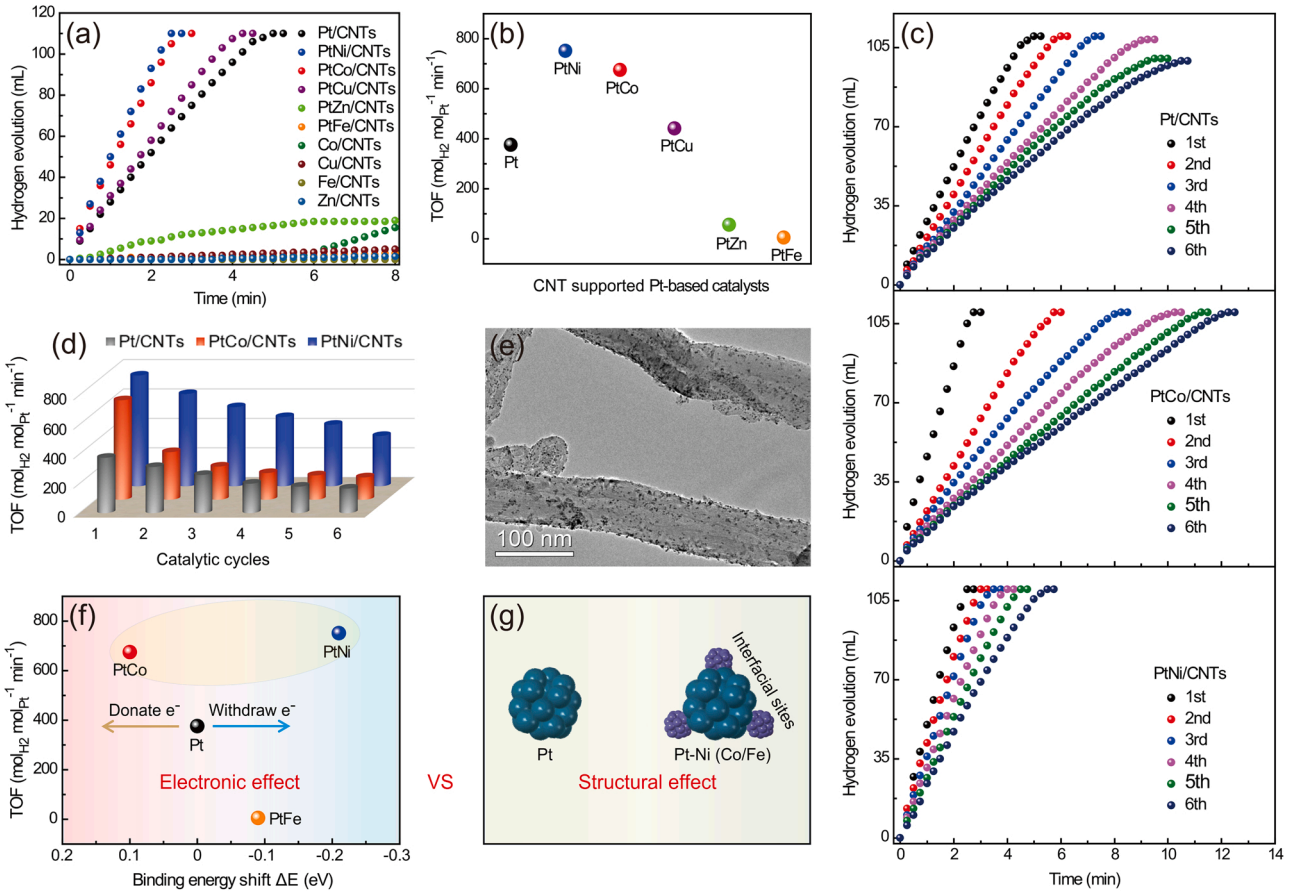

Fig. 6. (a) Volume of hydrogen evolved versus reaction time for hydrolytic dehydrogenation of AB at 25 °C catalyzed by the catalysts. (b) The comparison of TOF values of the Pt-based catalysts. (c,d) Durability results of the three catalysts. (e) The corresponding TEM image of the PtNi/CNTs catalysts after six catalytic cycles. The electronic (f) and structural (g) effects of Pt on the influence of catalytic activity. The number of the metal oxide ALD cycles is 20 unless otherwise specified.

3.3. DFT calculations

DFT calculations were then performed to probe the synergistic catalytic nature of the Pt-Ni and the role of the interfacial sites for the enhancement mechanism. From the above isotopic experiments, the cleavage of O-H bond in H_2O molecule is involved in the RDS for the catalytic hydrolysis reaction of AB. Therefore the adsorption and dissociation of the H_2O molecule on Pt(111) and the Ni-cluster/Pt(111) interface were firstly investigated by the DFT calculations (Figs. S12 and S13). As shown in Fig. 7a, the adsorption of H_2O molecule on the Ni-cluster/Pt(111) interface (−0.675 eV) is much stronger than that on Pt (111) (−0.213 eV), and the elongation of the O-H bond in H_2O molecule is also larger on the Ni-cluster/Pt(111) interface (0.983 Å) compared with that on Pt(111) (0.979 Å). The enhanced adsorption and activation of H_2O molecule on the Ni-cluster/Pt(111) interface could promote the dissociation of H_2O molecule, which can be further verified by calculating the dissociation reaction energy of H_2O molecule (Fig. 7b). The dissociation barrier of H_2O molecule on the Ni-cluster/Pt(111) interface is 0.61 eV, which is obviously lower than that on Pt(111) (0.95 eV). Interestingly, the dissociation of H_2O molecule on the Ni-cluster/Pt (111) interface is an exothermic process, while the dissociation of H_2O molecule on Pt(111) is an endothermic process. These results confirm that the Ni-cluster/Pt(111) interface is more favorable in both kinetics and thermodynamics for the dissociation of H_2O molecule. The enhanced adsorption and dissociation of H_2O molecule on the Ni-cluster/Pt(111) interface could be ascribed to the higher position of d-band center of the Pt-Ni interfacial sites(−1.07 eV) compared with the Pt sites(−1.95 eV) on Pt(111) surface (Fig. 7c and d). This results in the obviously enhanced redistribution of the charge density of H_2O molecule on the Ni-cluster/Pt(111) interface (Fig. 7e and f) and efficiently weakens the O-H bond. Furthermore, in order to investigate the desorption of H_2 products, the adsorption energy of H atom on Pt(111) and the Ni-cluster/Pt(111) interface (Fig. S14) were also calculated, and the result indicates that the adsorption strength of H atom on the Ni-cluster/Pt(111) interface (−0.381 eV) is relatively weaker compared with that on Pt(111) (−0.475 eV). This is because that H atom is adsorbed on the bridge site between Pt and Ni, and the synergistic effect of the two metals weakens the adsorption strength of H and correspondingly enhances the desorption capability of H_2 molecules [49,50]. This should be another reason for the significantly enhanced H_2 evolution activity of the PtNi/CNTs catalysts.

3.4. Pt-Ni synergistic catalytic mechanisms

Based on the results and analyses above, the possible enhancement mechanism is proposed. For the AB hydrolysis reaction, the catalytic performance is greatly influenced by the activation of AB and H_2O reactants. For the Pt metal nanoparticles with optimized size, the activation of AB on Pt is relatively easy because the hydrolysis of AB is a pseudo zero-order reaction toward the AB concentration. While its capability to activate H_2O, being the RDS, is relatively poor (Fig. 8b) [15]. The decoration of nickel species on Pt constructing the unique and highly active Pt-Ni interfaces could promote the dissociation of H_2O molecules being the RDS, compensating for the poor capability of Pt for H_2O dissociation, which synergistically contributes to the significant enhancement of hydrogen evolution activity and durability (Fig. 8b). More specifically, during the initial stage of the reaction, Pt metal is the main active sites generating the intermediates of active spillover

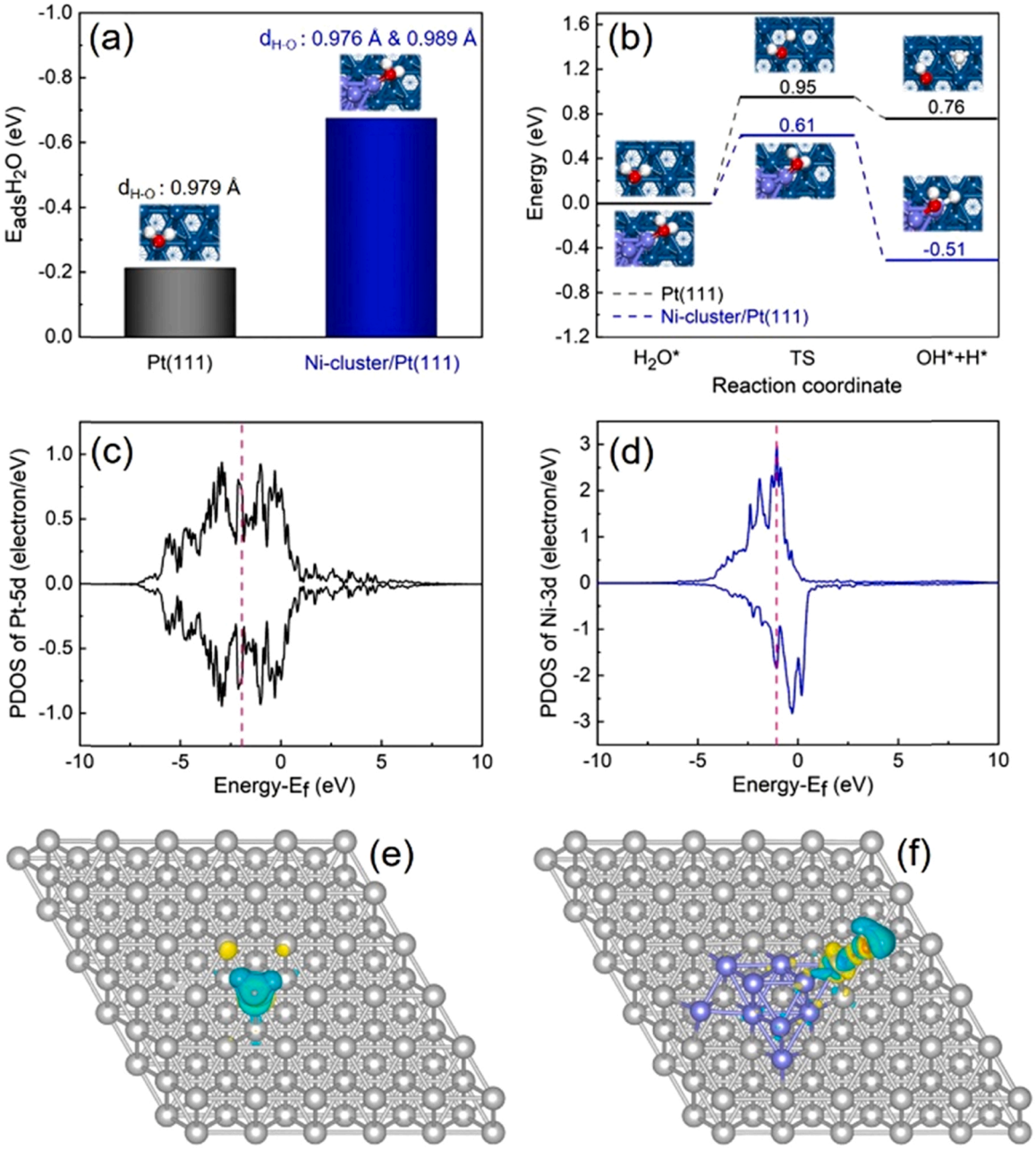

Fig. 7. (a) The calculated adsorption energy and O-H bond length of H_2O molecules on Pt(111) and Ni-cluster/Pt(111) interface. (b) The dissociation reaction energy profiles of H_2O molecule on Pt(111) and Ni-cluster/Pt(111) interface. The partial density of state (PDOS) diagrams of the d orbitals for the (c) Pt site on Pt(111) and (d) Ni site on the Ni-cluster/Pt(111) interface. The charge density differences of H_2O molecule on the (e) Pt site of Pt(111) and (f) Ni site of the Ni-cluster/Pt(111) interface (the yellow and cyan isosurfaces indicate the increase and decrease of 0.002 e/Å, respectively).

hydrogen (H·) because NiO is nearly inactive. Partial H· is reduced/combined to H_2 and desorbs from the Pt surfaces, and meanwhile a limited amount of H· spillovers to NiO resulting in the reduction of NiO to the nickel species with lower valent states (e.g., metallic Ni) [51]. The recycled PtNi100/CNTs catalysts present the magnetic separation property (Fig. S15), demonstrating that the NiO is indeed reduced to the metallic Ni by the active spillover H· during the in-situ reaction process. The in-situ formed metallic Ni could also act as the new active sites for the hydrogen evolution reaction to a certain extent (Fig. 8a). Once the metallic Ni is formed, the activation and dissociation of H_2O molecules being the RDS is greatly accelerated due to the strong capability of the Pt-Ni interfacial sites to adsorb, activate and dissociate H_2O molecules, and the weaker adsorption ability toward product molecules H_2. Besides, the addition of nickel species could inhibit the agglomeration and deformation of Pt nanoparticles improving the cycle performance of the PtNi/CNTs catalysts (Fig. 6c-e). All these factors synergistically afford the remarkably enhanced catalytic performances of the PtNi/CNTs catalysts. Considering the trade-off between the price and performance of noble and non-noble metal catalysts, single-atom alloy catalyst should be a promising choice for the hydrolytic generation of H_2, because it can not only maximize the atom-utilization efficiency of noble metal with low content, but also effectively utilize the bimetal synergy to modulating the catalytic performances [20].

In fact, the synergistic effects between Pt and Ni can also be verified in the selective hydrogenation of 5-hydroxymethylfurfural (HMF) to 2,5-bis(hydroxymethyl)furan (BHMF), which is a versatile and vital building block for the synthesis of resins, drugs and polymers (Fig. 8c) [52]. When using monometallic Pt/CNTs as catalysts, the conversion of

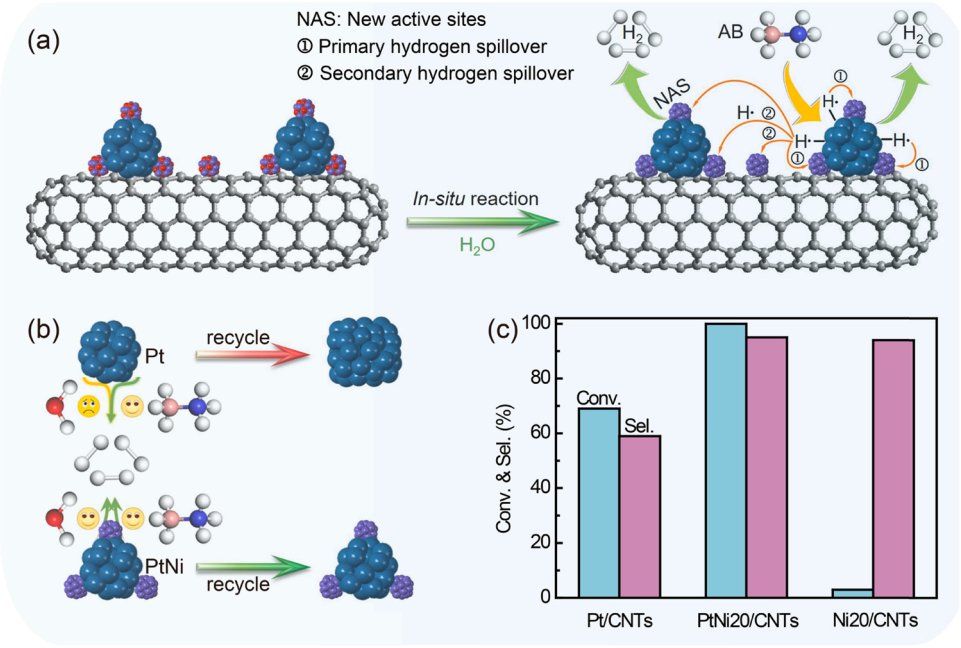

Fig. 8. (a) The proposed reaction mechanisms over the PtNi/CNTs catalysts. (b) Schematic illustration for H_2 evolution activity and durability over the Pt/CNTs and PtNi/CNTs catalysts. (c) The selective hydrogenation results of HMF to BHMF over the three catalysts.

HMF and selectivity to the targeted BHMF are approximately 69% and 59%, respectively. While the HMF reactants have been completely converted and the corresponding selectivity has been enhanced to 95% with the typical bimetal PtNi20/CNTs as catalysts. The addition of low oxophilic nickel species constructs the highly active Pt-Ni interfacial sites increasing the dissociation capability of H_2, which contributes to the selective hydrogenation of C═O and inhibits the dehydroxylation of BHMF because the PtNi bimetals with lower oxophilicity increase the energy barrier for direct C-O bond cleavage and lower the hydrogenation barrier as well, resulting in the remarkably enhanced activity and selectivity over the PtNi20/CNTs catalysts [53]. Similarly, the control experiments using Ni20/CNTs as catalysts show that the catalysts give poor activity (ca. 3% conversion). The selective hydrogenation results again confirm the remarkable synergy between Pt and Ni, which could be potentially applied in other heterocatalytic reactions.

4. Conclusions

In summary, we have successfully synthesized the highly efficient and durable PtNi/CNTs catalysts with ultrafine particle size and controllable interfacial sites by ALD technique. The decoration of nickel species on Pt lowers the reaction activation energy and compensates for the poor capability of Pt for H_2O molecule adsorption, activation and dissociation being the RDS for the AB hydrolysis reaction, correspondingly resulting in the significant enhancement of TOF value up to 751.6 mol_{H2} mol_{Pt}^{-1} min^{-1} for the optimized PtNi/CNTs catalysts and the obvious improvement of durability of the catalysts due to the remarkable Pt-Ni synergy. Experimental and theoretical results reveal that the constructed Pt-Ni interfacial sites could promote the adsorption, activation and dissociation of H_2O molecules and facilitate the desorption of H_2 molecules. Our study highlights the significance of tuning the interfacial structure in bimetal catalysts, and opens up an alternative avenue for the rational design of bimetal catalysts with optimal synergistic catalytic performances.

CRediT authorship contribution statement

Jiankang Zhang: Investigation, Visualization, Conceptualization, Supervision, Writing – review & editing, Funding acquisition. **Xiuhui Zheng:** Investigation, Formal analysis. **Wenlong Yu:** Formal analysis. **Xiang Feng:** Writing – review & editing, Supervision. **Yong Qin:** Writing – review & editing.

Declaration of Competing Interest

The authors declare that they have no known competing financial interests or personal relationships that could have appeared to influence the work reported in this paper.

Acknowledgements

We appreciate the financial support from the National Nature Science Foundation of China (22102131), National Postdoctoral Program for Innovative Talents (BX20180323), China Postdoctoral Science Foundation (2019M650169), Natural Science Foundation of Shandong Province (ZR2019BB039), Natural Science Basic Research Plan in Shaanxi Province of China (2021JQ-090), and the Fundamental Research Funds for the Central Universities (G2021KY05103). We would like to thank the Shanghai Synchrotron Radiation Facility for XAFS, and Analytical & Testing Center of Northwestern Polytechnical University for HAADF-STEM.

Appendix A. Supporting information

Supplementary data associated with this article can be found in the online version at doi:10.1016/j.apcatb.2022.121116.

References

[1] X. Zhang, M. Zhang, Y. Deng, M. Xu, L. Artiglia, W. Wen, R. Gao, B. Chen, S. Yao, X. Zhang, M. Peng, J. Yan, A. Li, Z. Jiang, X. Gao, S. Cao, C. Yang, A.J. Kropf, J. Shi, J. Xie, M. Bi, J.A. van Bokhoven, Y.-W. Li, X. Wen, M. Flytzani-Stephanopoulos, C. Shi, W. Zhou, D. Ma, A stable low-temperature H_2-production catalyst by crowding Pt on α-MoC, Nature 589 (2021) 396–401.
[2] M.A. Khalily, H. Eren, S. Akbayrak, H.H. Susapto, N. Biyikli, S. Özkar, M.O. Guler, Facile synthesis of three-dimensional Pt-TiO_2 nano-networks: a highly active catalyst for the hydrolytic dehydrogenation of ammonia-borane, Angew. Chem. Int. Ed. 128 (2016) 12445–12449.

[3] L. Zhang, K. Doyle-Davis, X. Sun, Pt-based electrocatalysts with high atom utilization efficiency: from nanostructures to single atoms, Energy Environ. Sci. 12 (2019) 492–517.
[4] A. Aijaz, A. Karkamkar, Y.J. Choi, N. Tsumori, E. Rönnebro, T. Autrey, H. Shioyama, Q. Xu, immobilizing highly catalytically active Pt nanoparticles inside the pores of metal-organic framework: a double solvents approach, J. Am. Chem. Soc. 134 (2012) 13926–13929.
[5] W. Chen, J. Ji, X. Feng, X. Duan, G. Qian, P. Li, X. Zhou, D. Chen, W. Yuan, Mechanistic insight into size-dependent activity and durability in Pt/CNT catalyzed hydrolytic dehydrogenation of ammonia borane, J. Am. Chem. Soc. 136 (2014) 16736–16739.
[6] L. Bai, X. Wang, C. Qiang, Y. Ye, H. Zheng, J. Guo, Y. Yin, C. Gao, Explaining the size dependence in platinum-nanoparticle-catalyzed hydrogenation reactions, Angew. Chem. Int. Ed. 55 (2016) 15656–15661.
[7] J. Knossalla, P. Paciok, D. Göhl, D. Jalalpoor, E. Pizzutilo, A.M. Mingers, M. Heggen, R.E. Dunin-Borkowski, K.J. Mayrhofer, F. Schüth, Shape-controlled nanoparticles in pore-confined space, J. Am. Chem. Soc. 140 (2018) 15684–15689.
[8] L. Liu, A. Corma, Metal catalysts for heterogeneous catalysis: from single atoms to nanoclusters and nanoparticles, Chem. Rev. 118 (2018) 4981–5079.
[9] J. Yang, W. Fu, C. Chen, W. Chen, W. Huang, R. Yang, Q. Kong, B. Zhang, J. Zhao, C. Chen, J. Luo, F. Yang, X. Duan, Z. Jiang, Y. Qin, Atomic design and fine-tuning of subnanometric Pt catalysts to tame hydrogen generation, ACS Catal. 11 (2021) 4146–4156.
[10] W. Yu, M.D. Porosoff, J.G. Chen, Review of Pt-based bimetallic catalysis: from model surfaces to supported catalysts, Chem. Rev. 112 (2012) 5780–5817.
[11] Y. Cao, Z. Sui, Y. Zhu, X. Zhou, D. Chen, Selective hydrogenation of acetylene over Pd-In/Al_2O_3 catalyst: promotional effect of indium and composition-dependent performance, ACS Catal. 7 (2017) 7835–7846.
[12] F. Fu, C. Wang, Q. Wang, A. Martinez-Villacorta, A. Escobar, H. Chong, X. Wang, S. Moya, L. Salmon, E. Fouquet, J. Ruiz, D. Astruc, Highly selective and sharp volcano-type synergistic Ni_2Pt@ZIF-8-catalyzed hydrogen evolution from ammonia borane hydrolysis, J. Am. Chem. Soc. 140 (2018) 10034–10042.
[13] X.-B. Zhang, J.-M. Yan, S. Han, H. Shioyama, Q. Xu, Magnetically recyclable Fe@Pt core-shell nanoparticles and their use as electrocatalysts for ammonia borane oxidation: the role of crystallinity of the core, J. Am. Chem. Soc. 131 (2009) 2778–2779.
[14] X. Yang, F. Cheng, J. Liang, Z. Tao, J. Chen, Pt_xNi_{1-x} nanoparticles as catalysts for hydrogen generation from hydrolysis of ammonia borane, Int. J. Hydrog. Energy 34 (2009) 8785–8791.
[15] W. Chen, W. Zheng, J. Cao, W. Fu, G. Qian, D. Chen, X. Zhou, X. Duan, Atomic insights into robust Pt-PdO interfacial site-boosted hydrogen generation, ACS Catal. 10 (2020) 11417–11429.
[16] W. Chen, D. Li, C. Peng, G. Qian, X. Duan, D. Chen, X. Zhou, Mechanistic and kinetic insights into the Pt-Ru synergy during hydrogen generation from ammonia borane over PtRu/CNT nanocatalysts, J. Catal. 356 (2017) 186–196.
[17] Z. Li, T. He, D. Matsumura, S. Miao, A. Wu, L. Liu, G. Wu, P. Chen, Atomically dispersed Pt on the surface of Ni particles: synthesis and catalytic function in hydrogen generation from aqueous ammonia-borane, ACS Catal. 7 (2017) 6762–6769.
[18] S. Wang, D. Zhang, Y. Ma, H. Zhang, J. Gao, Y. Nie, X. Sun, Aqueous solution synthesis of Pt-M (M = Fe, Co, Ni) bimetallic nanoparticles and their catalysis for the hydrolytic dehydrogenation of ammonia borane, ACS Appl. Mater. Interfaces 6 (2014) 12429–12435.
[19] Y. Cao, H. Zhang, S. Ji, Z. Sui, Z. Jiang, D. Wang, F. Zaera, X. Zhou, X. Duan, Y. Li, Adsorption site regulation to guide atomic design of Ni-Ga catalysts for acetylene semi-hydrogenation, Angew. Chem. Int. Ed. 132 (2020) 11744–11749.
[20] G. Giannakakis, M. Flytzani-Stephanopoulos, E.C.H. Sykes, Single-atom alloys as a eductionist approach to the rational design of heterogeneous catalysts, Acc. Chem. Res. 52 (2019) 237–247.
[21] J. Zhang, W. Chen, H. Ge, C. Chen, W. Yan, Z. Gao, J. Gan, B. Zhang, X. Duan, Y. Qin, Synergistic effects in atomic-layer-deposited PtCox/CNTs catalysts enhancing hydrolytic dehydrogenation of ammonia borane, Appl. Catal. B Environ. 235 (2018) 256–263.
[22] J. Zhang, Z. Yu, Z. Gao, H. Ge, S. Zhao, C. Chen, S. Chen, X. Tong, M. Wang, Z. Zheng, Y. Qin, Porous TiO_2 nanotubes with spatially separated platinum and CoO_x cocatalysts produced by atomic layer deposition for photocatalytic hydrogen, Angew. Chem. Int. Ed. 56 (2017) 816–820.
[23] L. Zhang, R. Si, H. Liu, N. Chen, Q. Wang, K. Adair1, Z. Wang, J. Chen, Z. Song, J. Li, M.N. Banis, R. Li, T.K. Sham, M. Gu, L. Liu, G.A. Botton, X. Sun, Atomic layer deposited Pt-Ru dual-metal dimers and identifying their active sites for hydrogen evolution reaction, Nat. Commun. 10 (2019) 4936.
[24] Z. Gao, Y. Qin, Design and properties of confined nanocatalysts by atomic layer deposition, Acc. Chem. Res. 50 (2017) 2309–2316.
[25] R.K. Ramachandran, J. Dendooven, M. Filez, V.V. Galvita, H. Poelman, E. Solano, M.M. Minjauw, K. Devloo-Casier, E. Fonda, D. Hermida-Merino, Atomic layer deposition route to tailor nanoalloys of noble and non-noble metals, ACS Nano 10 (2016) 8770–8777.
[26] X. Liu, Q. Zhu, Y. Lang, K. Cao, S. Chu, B. Shan, R. Chen, Oxide-nanotrap-anchored platinum nanoparticles with high activity and sintering resistance by area-selective atomic layer deposition, Angew. Chem. Int. Ed. 129 (2017) 1670–1674.
[27] B.J. O'Neill, D.H. Jackson, J. Lee, C. Canlas, P.C. Stair, C.L. Marshall, J.W. Elam, T. F. Kuech, J.A. Dumesic, G.W. Huber, Catalyst design with atomic layer deposition, ACS Catal. 5 (2015) 1804–1825.
[28] J.A. Singh, N. Yang, S.F. Bent, Nanoengineering heterogeneous catalysts by atomic layer deposition, Annu. Rev. Chem. Biomol. Eng. 8 (2017) 41–62.
[29] X. Meng, X. Wang, D. Geng, C. Ozgit-Akgun, N. Schneider, J.W. Elam, Atomic layer deposition for nanomaterial synthesis and functionalization in energy technology, Mater. Horiz. 4 (2017) 133–154.
[30] J. Lu, J.W. Elam, P.C. Stair, Synthesis and stabilization of supported metal catalysts by atomic layer deposition, Acc. Chem. Res. 46 (2013) 1806–1815.
[31] J. Zhang, Z. Gao, S. Wang, G. Wang, X. Gao, B. Zhang, S. Xing, S. Zhao, Y. Qin, Origin of synergistic effects in bicomponent cobalt oxide-platinum catalysts for selective hydrogenation reaction, Nat. Commun. 10 (2019) 4166.
[32] H. Yan, K. He, I.A. Samek, D. Jing, M.G. Nanda, P.C. Stair, J.M. Notestein, Tandem In_2O_3-Pt/Al_2O_3 catalyst for coupling of propane dehydrogenation to selective H_2 combustion, Science 371 (2021) 1257–1260.
[33] J. Zhao, C. Chen, B. Zhang, Z. Jiao, J. Zhang, J. Yang, Y. Qin, Tuning the selectivity of Pt-catalyzed tandem hydrogenation of nitro compounds via controllable NiO decoration by atomic layer deposition, Catal. Commun. 121 (2019) 48–52.
[34] Y. Peng, Y. He, Y. Wang, Y. Long, G. Fan, Sustainable one-pot construction of oxygen-rich nitrogen-doped carbon nanosheets stabilized ultrafine Rh nanoparticles for efficient ammonia borane hydrolysis, J. Colloid Interface Sci. 594 (2021) 131–140.
[35] W. Wang, Z.H. Lu, Y. Luo, A. Zou, Q. Yao, X. Chen, Mesoporous carbon nitride supported Pd and Pd-Ni nanoparticles as highly efficient catalyst for catalytic hydrolysis of NH_3BH_3, ChemCatChem 10 (2018) 1620–1626.
[36] X. Huang, Y. Liu, H. Wen, R. Shen, S. Mehdi, X. Wua, E. Liang, X. Guo, B. Li, Ensemble-boosting effect of Ru-Cu alloy on catalytic activity towards hydrogen evolution in ammonia borane hydrolysis, Appl. Catal. B Environ. 287 (2021), 119960.
[37] J. Li, Q. Guan, H. Wu, W. Liu, Y. Lin, Z. Sun, X. Ye, X. Zheng, H. Pan, J. Zhu, S. Chen, W. Zhang, S. Wei, J. Lu, Highly active and stable metal single-atom catalysts achieved by strong electronic metal-support interactions, J. Am. Chem. Soc. 141 (2019) 14515–14519.
[38] S. Özkar, A review on platinum(0) nanocatalysts for hydrogen generation from the hydrolysis of ammonia borane, Dalton Trans. 50 (2021) 12349–12364.
[39] M. Zahmakiran, S. Özkar, Transition metal nanoparticles in catalysis for the hydrogen generation from the hydrolysis of ammonia-borane, Top. Catal. 56 (2013) 1171–1183.
[40] W.-W. Zhan, Q.-L. Zhu, Q. Xu, Dehydrogenation of ammonia borane by metal nanoparticle catalysts, ACS Catal. 6 (2016) 6892–6905.
[41] C. Mboyi, D. Poinsot, J. Roger, K. Fajerwerg, M. Kahn, J.-C. Hierso, The hydrogen-storage challenge: nanoparticles for metal-catalyzed ammonia borane dehydrogenation, Small 17 (2021), 2102759.
[42] U.B. Demirci, Ammonia borane, a material with exceptional properties for chemical hydrogen storage, Int. J. Hydrog. Energy 42 (2017) 9978–10013.
[43] C.Y. Alpaydın, S.K. Gülbay, C.O. Colpan, A review on the catalysts used for hydrogen production from ammonia borane, Int. J. Hydrog. Energy 45 (2020) 3414–3434.
[44] P. Verma, K. Yuan, Y. Kuwahara, K. Mori, H. Yamashita, Enhancement of plasmonic activity by Pt/Ag bimetallic nanocatalyst supported on mesoporous silica in the hydrogen production from hydrogen storage material, Appl. Catal. B Environ. 223 (2018) 10–15.
[45] L. Wang, H. Li, W. Zhang, X. Zhao, J. Qiu, A. Li, X. Zheng, Z. Hu, R. Si, J. Zeng, Supported rhodium catalysts for ammonia-borane hydrolysis: dependence of the catalytic activity on the highest occupied state of the single rhodium atoms, Angew. Chem. Int. Ed. 56 (2017) 4712–4718.
[46] P. Li, R. Chen, S. Zhao, W. Li, Y. Lin, Y. Yu, Architecture control and electronic structure engineering over Ni-based nitride nanocomposite for boosting ammonia borane dehydrogenation, Appl. Catal. B Environ. 298 (2021), 120523.
[47] P.C. Stair, Where the action is, Nat. Chem. 3 (2011) 345–346.
[48] H. Yan, S. Yao, J. Wang, S. Zhao, Y. Sun, M. Liu, X. Zhou, G. Zhang, X. Jin, X. Feng, Y. Liu, X. Chen, D. Chen, C. Yang, Engineering Pt-Mn_2O_3 interface to boost selective oxidation of ethylene glycol to glycolic acid, Appl. Catal. B Environ. 284 (2021), 119803.
[49] J.R. Kitchin, N.A. Khan, M.A. Barteau, J.G. Chen, B. Yakshinskiy, T.E. Madey, Elucidation of the active surface and origin of the weak metal-hydrogen bond on Ni/Pt (111) bimetallic surfaces: a surface science and density functional theory study, Surf. Sci. 544 (2003) 295–308.
[50] M.P. Humbert, J.G. Chen, Correlating hydrogenation activity with binding energies of hydrogen and cyclohexene on M/Pt(111) (M= Fe, Co, Ni, Cu) bimetallic surfaces, J. Catal. 257 (2008) 297–306.
[51] M. Xiong, Z. Gao, Y. Qin, Spillover in heterogeneous catalysis: new insights and opportunities, ACS Catal. 11 (2021) 3159–3172.
[52] Y. Li, X. Zhang, N. Li, P. Xu, W. Lou, M. Zong, Biocatalytic reduction of HMF to 2,5-bis(hydroxymethyl)furan by HMF-tolerant whole cells, ChemSusChem 10 (2017) 372–378.
[53] X. Wang, M. Arai, Q. Wu, C. Zhang, F. Zhao, Hydrodeoxygenation of lignin-derived phenolics-a review on the active sites of supported metal catalysts, Green Chem. 22 (2020) 8140–8168.